Inorganic Chemistry

Article

pubs.acs.org/IC

Equilibrium, Kinetic, and Computational Studies on the Formation of Cu^{2+} and Zn^{2+} Complexes with an Indazole-Containing Azamacrocyclic Scorpiand: Evidence for Metal-Induced Tautomerism

Begoña Verdejo,*[,†] Laura Acosta-Rueda,[‡] M. Paz Clares,[†] Almudena Aguinaco,[‡] Manuel G. Basallote,*[,‡] Concepción Soriano,[§] Roberto Tejero,[∥] and Enrique García-España*[,†]

[†]Instituto de Ciencia Molecular, C/Catedrático José Beltrán 2, 46980 Paterna, Valencia, Spain

[‡]Dpto. Ciencia de los Materiales e Ingeniería Metalúrgica y Química Inorgánica, Facultad de Ciencias, Universidad de Cádiz, Avenida República Saharahui s/n, 11510, Puerto Real, Cádiz, Spain

[§]Departamento de Química Orgánica, Facultad de Farmacia, Universidad de Valencia, C/Vicente Andrés Estellés s/n, 46100 Burjassot, Valencia, Spain

[∥]Departamento de Química Física, Universidad de Valencia, C/Dr. Moliner s/n, 46100 Burjassot, Valencia, Spain

Supporting Information

ABSTRACT: Cu^{2+} and Zn^{2+} coordination chemistry of a new member of the family of scorpiand-like macrocyclic ligands derived from tris(2-aminoethyl)amine (*tren*) is reported. The new ligand (**L1**) contains in its pendant arm not only the amine group derived from *tren* but also a 6-indazole ring. Potentiometric studies allow the determination of four protonation constants. UV−vis and fluorescence data support that the last protonation step occurs on the indazole group. Equilibrium measurements in the presence of Cu^{2+} and Zn^{2+} reveal the formation of stable $[ML1]^{2+}$, $[MHL1]^{3+}$, and $[ML1(OH)]^{+}$ complexes. Kinetic studies on the acid-promoted decomposition of the metal complexes were carried out using both absorbance and fluorescence detection. For Zn^{2+}, both types of detection led to the same results. The experiments suggest that $[ZnL1]^{2+}$ protonates upon addition of an acid excess to form $[ZnHL1]^{3+}$ within the mixing time of the stopped-flow instrument, which then decomposes with a first-order dependence on the acid concentration. The kinetic behavior is more complex in the case of Cu^{2+}. Both $[CuL1]^{2+}$ and $[CuHL1]^{3+}$ show similar absorption spectra and convert within the mixing time to a new intermediate species with a band at 750 nm, the process being reverted by addition of base. The intermediate then decomposes with a second-order dependence on the acid concentration. However, kinetic experiments with fluorescence detection showed the existence of an additional faster step. With the help of DFT calculations, an interpretation is proposed in which protonation of $[CuL1]^{2+}$ to form $[CuHL1]^{3+}$ would involve dissociation of the *tren*-based NH group in the pendant arm and coordination of a 2*H*-indazole group. Further protonation would lead to dissociation of coordinated indazole, which then will convert to the more stable 1*H* tautomer in a process signaled by fluorescence changes that would not be affecting to the d−d spectrum of the complex.

INTRODUCTION

Macrocyclic ligands with a pendant arm containing a donor atom (scorpiand-like ligands) are able to undergo conformational reorganizations in which the pendant arm folds toward or separates from the macrocyclic core in response to chemical stimuli.[1] Although such movements are facilitated in the complexes by the presence of a metal center, we have shown that they can also occur in the ligand itself as a consequence of variations in the hydrogen bonding network and $\pi-\pi$ stacking brought about by changes in the protonation state.[2] In metal complexes, the coordination/dissociation of the donor atom in the pendant arm is also promoted by pH changes. As there is the possibility that, on the one hand, the biological activity of these compounds could be, in part, related to this movement,[3] and that, on the other hand, the movement itself could promote changes in the availability of chemical groups in the arm, we decided to explore the properties of scorpiands containing in the arm groups that might also display biological activity by themselves. In this regard, the indazole ring is of great interest due to the wide variety of pharmacological implications observed for its derivatives, such as anti-inflammatory, antimicrobial, antihypertensive, antiprotozoal, or antiobesity activities.[4] Moreover, recently, a ruthenium indazole complex has shown interesting perspectives as an antitumoral drug.[5] Nevertheless, indazole, also called benzpyrazole or isoindazone,[6] is a heterocyclic aromatic organic compound with a rare occurrence in nature. In fact, only three natural products containing an indazole ring have been isolated so far: nigellicine,[7] nigeglanine,[8] and nigellidine.[9] By considering

Received: December 4, 2014
Published: January 30, 2015

DOI: 10.1021/ic5029004
Inorg. Chem. 2015, 54, 1983−1991

exclusively the ring proton associated with the nitrogen, there are three different tautomers associated with this heterocycle (Chart 1). 1*H*-Indazole and its derivatives are usually

Chart 1

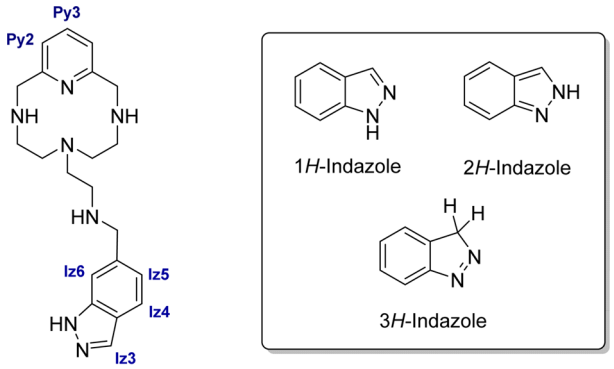

L1

thermodynamically stable, thus being the dominant tautomers vs the corresponding 2*H* and 3*H*-forms in the gas phase and in solution.[10] In agreement with the higher stability of the 1*H*-indazole tautomer, coordination to metal ions through N2 is the preferred binding mode, and examples have been widely reported in the literature.[11] However, only two examples of indazole coordination via N1 to transition metal ions have been reported in which their formation required tautomerization to the 2*H*-indazole form.[12]

Herein, we report on the synthesis of a new scorpiand-like ligand (**L1**) containing an indazole moiety in the pendant arm (Chart 1). Potentiometric, kinetic, and computational studies on the coordination complexes of **L1** with Cu^{2+} provide evidence for the existence of a structural reorganization that involves tautomerization, so that complex species with either the 1*H*- or 2*H*-forms are formed depending on the pH.

EXPERIMENTAL SECTION

Synthesis. The synthesis of **L1** has been carried out following the general procedure described for the preparation of **L2** (Chart 2),[2] which consists of the reaction of 6-(2-aminoethyl)-3,6,9-triaza-1(2,6)-pyridinacyclodecaphane (**L**) and the corresponding 1*H*-indazole-6-carboxaldehyde in ethanol, followed by reduction with sodium borohydride.

*6-[2-(N-Methyl-1H-indazol-6-yl)ethylamino]-3,6,9-triaza-1(2,6)-pyridinacyclodecaphane Hydrochloride (**L1**·3HCl·H_2O).* 6-(2-Aminoethyl)-3,6,9-triaza-1(2,6)-pyridinacyclodecaphane (0.60 g, 2.41 mmol) and 1*H*-indazole-6-carboxaldehyde (0.35 g, 2.41 mmol) were dissolved in 100 mL of dry ethanol and stirred at room temperature for 2 h. Then, sodium borohydride (0.91 g, 24.1 mmol) was added, and the stirring was maintained for 2 h more. Then, the solution was vacuum-evaporated and extracted with CH_2Cl_2/H_2O. The organic phase was taken to dryness and redissolved in dry ethanol. The hydrochloride salt of the product was precipitated by adding a concentrated hydrochloride acid solution. ^{1}H NMR (D_2O, 300 MHz): δ_H 2.79 (t, J = 5 Hz, J = 5.5 Hz, 4H), 2.96 (t, J = 7.8 Hz, 2H), 3.13 (t, J = 5 Hz, J = 4.1 Hz, 4H), 3.23 (t, J = 8.2 Hz, 2H), 4.32 (s, 2H), 4.51 (s, 4H), 7.16 (d, J = 8.2 Hz, 1H), 7.33 (d, J = 7.8 Hz, 1H), 7.64 (s, 1H), 7.82−7.86 (m, 2H), 8.08 (s, 1H). ^{13}C NMR (D_2O, 75.43 MHz): δ_C 42.5, 45.9, 49.4, 50.5, 50.8, 51.8, 112.5, 122.2 (2), 122.3, 123.0, 129.4, 134.3, 139.8, 140.0, 148.9. Anal.Calcd for $C_{21}H_{29}N_7$·3HCl·H_2O: C, 49.76; H, 6.76; N, 19.34. Found: C, 49.95, H, 6.78; N 19.24.

EMF Measurements. The potentiometric titrations were carried out at 298.1 ± 0.1 K using NaCl 0.15 M as supporting electrolyte. The

Chart 2

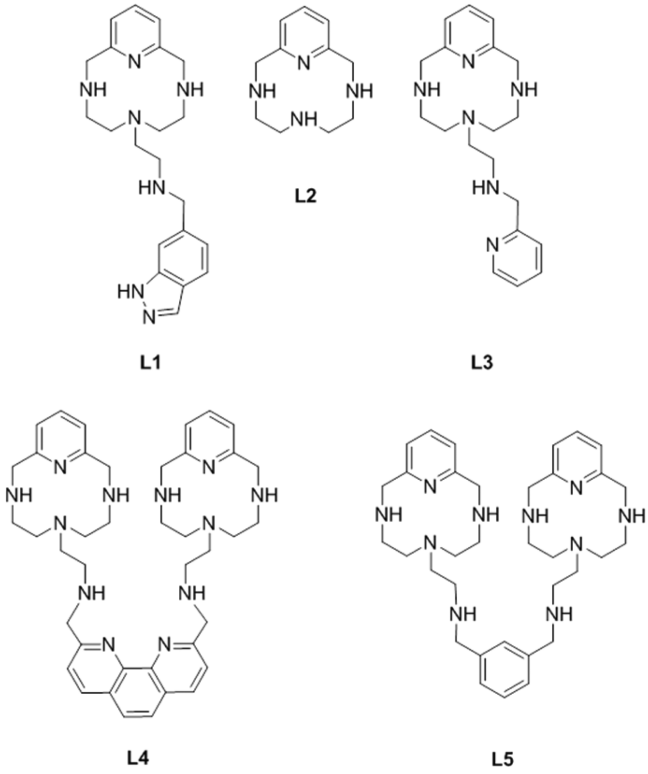

experimental procedure (burette, potentiometer, cell, stirrer, microcomputer, etc.) has been fully described elsewhere.[13] The acquisition of the emf data was performed with the computer program PASAT.[14] The reference electrode was an Ag/AgCl electrode in saturated KCl solution. The glass electrode was calibrated as a hydrogen-ion concentration probe by titration of previously standardized amounts of HCl with CO_2-free NaOH solutions and the equivalent point determined by Gran's Method,[15] which gives the standard potential, $E^{\circ\prime}$, and the ionic product of water (pK_w = 13.73(1)).

The computer program HYPERQUAD was used to calculate the protonation and stability constants.[16] The pH range investigated was 2.5−11.0, and the concentration of the metal ions and of the ligand ranged from 1×10^{-3} to 5×10^{-3} M with the M:L molar ratio varying from 2:1 to 1:2. The different titration curves for each system (at least two) were treated either as a single set or as separated curves without significant variations in the values of the stability constants. Finally, the sets of data were merged together and treated simultaneously to give the final stability constants.

NMR Measurements. The ^{1}H and ^{13}C NMR spectra were recorded on a Bruker Avance AC-300 spectrometer operating at 299.95 MHz for ^{1}H and at 75.43 MHz for ^{13}C. The chemical shifts are given in parts per million referenced to the solvent signal. Adjustments to the desired pH were made using drops of DCl or NaOD solutions. The pD was calculated from the measured pH values using the correlation, pH = pD − 0.4.[17]

Spectrophotometric and Spectrofluorimetric Titrations. Absorption spectra were recorded on a Shimadzu UV-2501 PC spectrophotometer. Fluorescence spectra were obtained with a PTI MO-5020 spectrofluorimeter. The emission spectra were measured from 300 to 500 nm for an excitation wavelength of 260 nm, corresponding to the maximum of the excitation intensity. HCl and NaOH were used to adjust the pH values that were measured with a Metrohm 713 pH meter in both cases.

Kinetic Experiments. The kinetic experiments were carried out at 298.1 ± 0.1 K with both a Cary 50-BIO spectrophotometer and an Applied Photophysics SX17MV stopped-flow instrument provided with different detectors: PDA-1 diode array, fluorescence, and absorbance. The ionic strength was adjusted to 0.15 M by adding

DOI: 10.1021/ic5029004
Inorg. Chem. 2015, 54, 1983−1991

the required amount of NaCl. The conventional or the stopped-flow spectrophotometers were used depending on the time scale of the different processes, but the data were in all cases analyzed with SPECFIT software.[18]

In the fluorescence experiments, both the absorbance and the fluorescence were simultaneously detected. Thus, the absorbance changes were registered at the excitation wavelength used, while the fluorescence changes correspond to the addition of signals obtained for all wavelengths longer than 295 nm. An FSR-WG295 filter provided by Newport was placed in the fluorescence detector to cut off any contribution from wavelengths below 295 nm.

The kinetic studies on complex decomposition were carried out under pseudo-first-order conditions of acid excess, and the solutions contained Cu^{2+} and the ligand in 1:1 molar ratio with the pH adjusted using NaOH and HCl solutions. Additionally, some experiments were carried out using a sodium formate/formic acid buffer solution at pH 4. In all cases, the equilibrium speciation curves were used to determine the composition of the solutions at the different pH values. Reversibility studies were performed adding HCl or NaOH to a solution containing Cu^{2+} and L in a 1:1 molar ratio.

Computational Aspects. All calculations carried out in this study were performed using the C.01 revision of the Gaussian 09 program package.[19] The MOLDEN[20] program was used in preprocessing, preparing the input structures and in the final stages of visualizing and analyzing the resulting geometries. Density functional theory calculations (DFT) using Becke's three-parameter B3LYP[21] functional with the mixed LANL2DZ (on the transition metal) and 6-311G(2d,p)[22] basis sets were performed. The B3LYP functional has become a standard in DFT and has been selected for our calculations, given its widespread use and reliability being also fairly robust.

RESULTS AND DISCUSSION

Acid–Base Behavior. Table 1 collects the stepwise protonation constants of **L1** obtained at 298.1 ± 0.1 K in 0.15 M NaCl, and Figure S1 (Supporting Information) collects the corresponding distribution diagram. **L1** presents four stepwise protonation constants in the pH range studied (2.0–11.0). The first three protonation steps, which occur at the secondary amino groups, have values close to those previously reported for the analogous derivatives with naphthalene, pyridine, anthracene, or quinoline moieties in the pendant arm.[2,3,24] The last protonation constant detected by potentiometry, which has a much lower value, can be assigned to the indazole amino group, as supported by UV–vis and fluorescence studies (vide infra).

Table 1. Logarithms of the Stepwise Protonation Constants for L1 Determined at 298.1 ± 0.1 K in 0.15 M NaCl

reaction[a]	L1
$H + L \rightleftharpoons HL$	9.94(1)[b]
$H + HL \rightleftharpoons H_2L$	8.73(1)
$H + H_2L \rightleftharpoons H_3L$	7.28(1)
$H + H_3L \rightleftharpoons H_4L$	1.88(9)
$\log \beta$[c]	27.8

[a]Charges have been omitted. [b]Numbers in parentheses are standard deviations in the last significant figure. [c]$\log \beta = \Sigma \log K_{HjL}$.

As occurs for other scorpiand-like ligands in which the pendant arm approaches or leaves the macrocyclic core as a result of a change in the protonation state,[2] the molecular rearrangement of **L1** is observed in the absence of transition metal ions. Regarding this point, the ^{1}H NMR spectra recorded at variable pH show that, on going from a pH level of 6 to 8, corresponding to the deprotonation of $[H_3\mathbf{L1}]^{3+}$ to give $[H_2\mathbf{L1}]^{2+}$, there is an upfield shift of all the aromatic signals of both the indazole and the pyridine, supporting the occurrence of stacking between them (Figure 1).

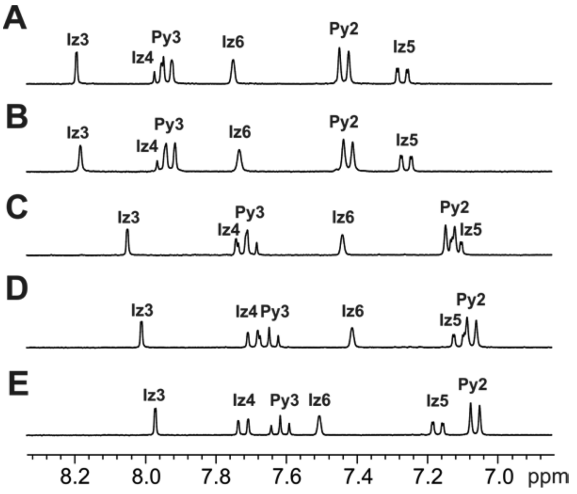

Figure 1. ^{1}H NMR spectra (aromatic region) in D_2O of **L1** recorded at (A) pD = 1.91; (B) pD = 5.60; (C) pD = 8.28; (D) pD = 9.34; (E) pD = 11.70. The spectra of the aliphatic region are shown in Figure S2 (Supporting Information).

Stacking is also evidenced by changes in the UV–vis spectra, which present two characteristic absorption bands (λ_{max} = 250–255 nm and λ_{max} = 285–290 nm) associated with $\pi \rightarrow \pi^*$ transitions in the indazole ring.[25] On moving from acidic to basic pH, the band centered at 250 nm experiences an increase in intensity and a bathochromic effect that can be ascribed to a charge-transfer band associated with the π–π stacking of the aromatic rings, pyridine and indazole. However, above pH 6, the absorption band centered at 290 nm undergoes the opposite effect with a decrease in intensity and a hypsochromic shift (Figure 2)

Furthermore, fluorescence emission spectra show a quenching effect when $[H_3\mathbf{L1}]^{3+}$ converts to $[H_2\mathbf{L1}]^{2+}$, denoting that deprotonation of the secondary amino group closest to the indazole fragment is occurring at this stage (Figure 3). This deprotonation makes operative a photoinduced electron transfer from the amine to the excited fluorophore, yielding a

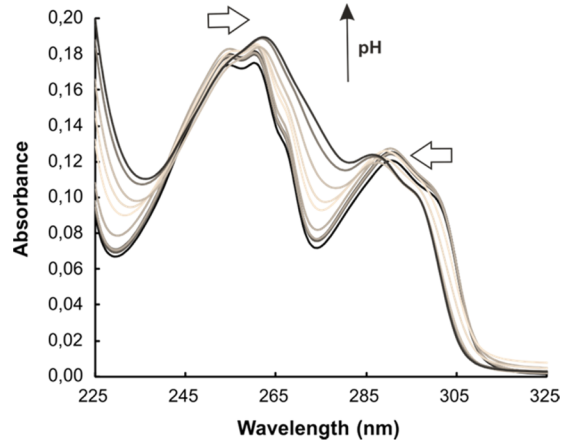

Figure 2. pH dependence of the absorption spectrum of **L1**. $[\mathbf{L1}]_0$ = 1.0×10^{-5} M.

DOI: 10.1021/ic5029004
Inorg. Chem. 2015, 54, 1983–1991

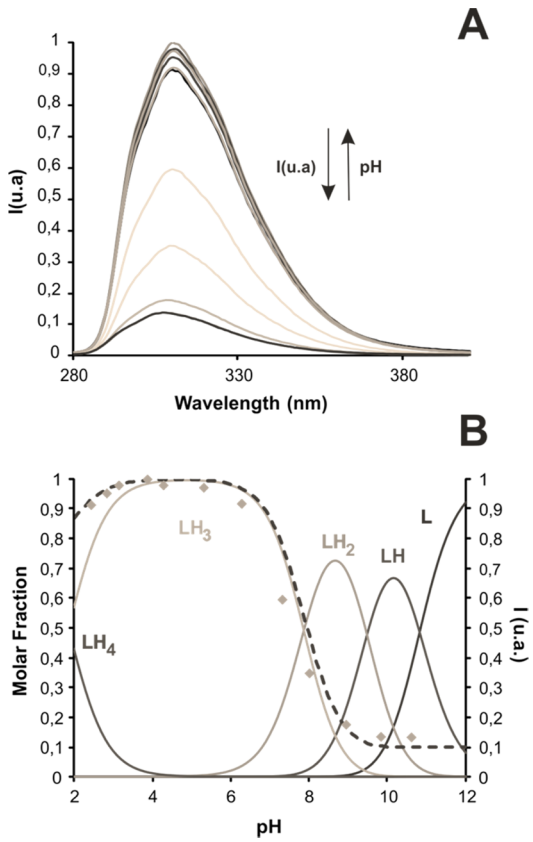

Figure 3. Fluorescence emission spectra of **L1** (λ_{exc} = 260 nm) recorded at 298.1 ± 0.1 K in 0.15 M NaCl at pH ranging between 2 and 11 with [**L1**] = 1.0 × 10^{-5} M. Steady-state fluorescence emission titration curve of **L1** (λ_{exc} = 260 nm) measured in 0.15 M NaCl at 298.1 ± 0.1 K with [**L1**] = 1.0 × 10^{-5} M (♦) and mole fraction distribution curves for the various protonated forms (solid lines).

quenching of the fluorescence. As occurs for other scorpiand-like ligands,[2,3,24] the observed quenching of the fluorescence is just partial. This incomplete quenching of the fluorescence could be explained taking as a reference the hydrogen bonding observed in the solid state for the analogous receptor with a naphthalene moiety that also persists in solution.[2] Hydrogen bonding between the amino group in the arm and the protonated secondary amino groups in the macrocyclic core would somehow block the electron pair of the amino group of the arm, hindering the electron transfer to the excited fluorophore and hence leaving a residual emission.

Cu^{2+} and Zn^{2+} Coordination. *EMF Studies.* Table 2 collects the stepwise stability constants for the interactions of **L1** with Cu^{2+} and Zn^{2+} determined in water at 298.1 ± 0.1 K in 0.15 M NaCl. Under these conditions, only mononuclear

Table 2. Logarithms of the Formation Constants (log *K*) of the Cu^{2+} and Zn^{2+} Complexes with L1 Determined at 298.1 ± 0.1 K in 0.15 M NaCl

reaction	Cu^{2+}	Zn^{2+}
M + L ⇌ ML[a]	19.42(1)[b]	16.75(1)
ML + H ⇌ MHL	3.82(3)	4.23(2)
ML + OH ⇌ ML(OH)	2.63(4)	2.33(5)

[a]Charges have been omitted. [b]Numbers in parentheses are standard deviations in the last significant figure.

$[MHL]^{3+}$, $[ML]^{2+}$, and $[ML(OH)]^{+}$ complexes were detected, the $[ML]^{2+}$ species being predominant over a wide pH range. It is interesting to note that the stability constants for the $[ML]^{2+}$ species are very similar to the values obtained for other scorpiand-like ligands in which the donor atom in the tail binds the metal ion.[2,3,23,24] A priori, the geometry adopted by the complex would prevent the implication of the 1*H*-indazole tautomer in the coordination to the metal complex. Comparison between the protonation constants of the $[ML]^{2+}$ complexes and the free ligand species with the same charge ($[CuL]^{2+} + H^{+} \rightleftharpoons [CuHL]^{3+}$, log *K* = 3.82, $[ZnL]^{2+} + H^{+} \rightleftharpoons [ZnHL]^{3+}$, log *K* = 4.23 vs $[H_2L]^{2+} + H^{+} \rightleftharpoons [H_3L]^{3+}$, log *K* = 7.28) shows a much higher value for the free ligand, suggesting that protonation of the $[ML]^{2+}$ complexes brings about the breakage of an M−N bond.[2]

Fluorescence Studies. Fluorescence emission studies of the Cu^{2+} complexes (Figure 4) reveal a strong quenching effect

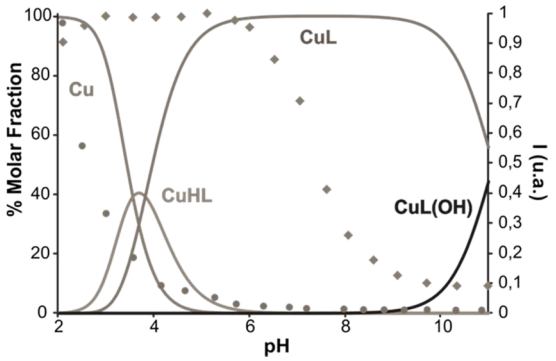

Figure 4. Steady-state fluorescence emission titration curve of Cu^{2+}-**L1** (●) and the corresponding free ligand (♦) measured in 0.15 M NaCl at 298.1 ± 0.1 K with [M^{2+}−**L1**] or [**L1**] = 1.0 × 10^{-5} M. The corresponding mole fraction distribution curves for Cu^{2+} and the various protonated forms of M^{2+}-L are shown as solid lines (λ_{exc} = 260 nm).

following the formation of the monoprotonated complex $[MHL]^{3+}$. This quenching is preserved for the species formed at neutral ($[ML]^{2+}$) and alkaline ($[ML(OH)]^{+}$) pH values.

However, a very different behavior was observed for the Zn^{2+} complexes (see Figure 5). In this system, an increase in the

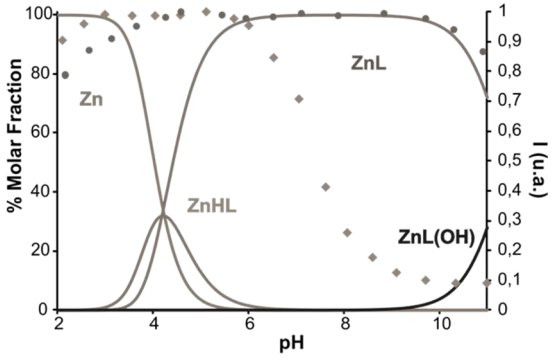

Figure 5. Steady-state fluorescence emission titration curve of Zn^{2+}-**L1** (●) and the corresponding free ligand (♦) measured in 0.15 M NaCl at 298.1 ± 0.1 K with [Zn^{2+}−**L1**] or [**L1**] = 1.0 × 10^{-5} M. The corresponding mole fraction distribution curves for Zn^{2+} and the various protonated forms of M^{2+}-L are shown as solid lines (λ_{exc} = 260 nm).

DOI: 10.1021/ic5029004
Inorg. Chem. 2015, 54, 1983−1991

fluorescence (chelation-enhanced fluorescence, CHEF) was observed above pH 6 in correspondence with the complexation of the metal ion. Coordination of the d^{10} Zn^{2+} by all the amino groups of the ligands blocks the lone pairs, preventing their photoinduced transfer to the LUMO orbitals of the fluorophore.[26] Furthermore, the formation of hydroxo-complexes above pH 10 is associated with a slight deactivation of the fluorescence.[27]

Kinetics of Decomposition of Zn^{2+} and Cu^{2+} Complexes. The species distribution curves obtained from the equilibrium constants were used to select the experimental conditions for the kinetic studies on complex decomposition. This kind of experiment has been previously reported to provide in certain cases information not only about the ligand dissociation process but also about structural reorganizations as those occurring in complexes with scorpiands and other related azacyclophanes.[2,28] To obtain more information on the kinetics of structural reorganizations, the experiments performed adding an excess of acid have been complemented with stopped-flow experiments in which buffers were used to change the pH of the solution between values corresponding to the formation of the different major species.

For the Zn^{2+} complexes, the speciation curves in Figure 5 show that Zn^{2+}-**L1** solutions in a 1:1 molar ratio only contain $[ZnL1]^{2+}$ at pH 8. Addition of a large excess of acid leads to complete complex decomposition, yielding Zn^{2+} and a mixture of $[H_3L1]^{3+}$ and $[H_4L1]^{4+}$. The kinetics of decomposition was studied under the same conditions of temperature and ionic strength used for the potentiometric studies, and the reaction was monitored at 270 nm, which is the wavelength with the largest difference between the absorptivities of the protonated ligand and of the $[ZnL1]^{2+}$ species (Figure 6). The absorbance

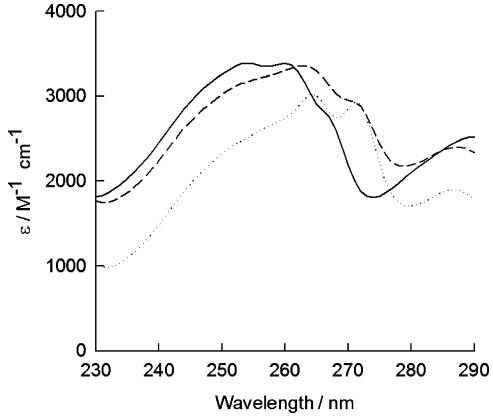

Figure 6. Absorption spectra of $ZnL1^{2+}$ (dashed line), $ZnHL1^{3+}$ (dotted line), and protonated ligand (continuous line). $[Zn^{2+}]_0$ = $[L1]_0$ = 1×10^{-4} M. The spectra were calculated from the spectra recorded at different pHs by using the percentages of the different species calculated with the equilibrium constants in Tables 1 and 2.

changes so obtained were fitted satisfactorily to a single exponential and yielded an observed rate constant that changes linearly with the acid concentration (Figure 7). The fit of the data to eq 1 leads to $a = (4.3 \pm 0.1)$ M^{-1} s^{-1}.

However, literature precedents[2,23,29] show that there is the possibility that the rate constants in Figure 7 actually correspond to decomposition of $[ZnHL1]^{3+}$, which could be formed in a rapid step occurring within the stopped-flow mixing time. To obtain information on this point, solutions of

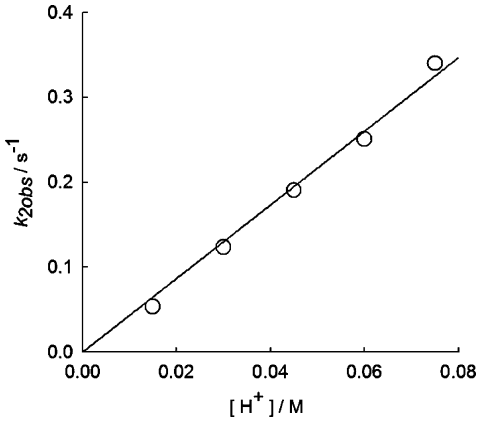

Figure 7. Plot of the dependence with the acid concentration of the observed rate constant obtained from the variation of absorbance during the acid-promoted decomposition of $[ZnL1]^{2+}$ species ([NaCl] = 0.15 M, 298.1 K).

Zn^{2+} and **L1** in a 1:1 molar ratio with the pH adjusted to 4 were mixed in the stopped-flow instrument with an acid excess, and results similar to those in Figure 7 were obtained (see Figure S3, Supporting Information), the value of the second-order rate constant being now $a = (4.25 \pm 0.06)$ M^{-1} s^{-1}. As solutions with an initial pH of 8 contain exclusively $[ZnL1]^{2+}$ and solutions at pH 4 contain a mixture of $[ZnL1]^{2+}$ and $[ZnHL1]^{3+}$, the results so obtained indicate that both Zn^{2+}-**L1** complexes decompose with the same kinetics. These results were confirmed by stopped-flow experiments with monitoring of fluorescence, which yielded second-order rate constants of $a = (4.0 \pm 0.1)$ M^{-1} s^{-1} for $[ZnL1]^{2+}$ and $a = (4.1 \pm 0.1)$ M^{-1} s^{-1} for the mixture of $[ZnL1]^{2+}$ and $[ZnHL1]^{3+}$ (Figures S4 and S5, Supporting Information). Thus, it appears that $[ZnL1]^{2+}$ protonates upon addition of an acid excess to form $[ZnHL1]^{3+}$ within the mixing time of the stopped-flow instrument, a behavior similar to that already reported for Cu^{2+} complexes with related scorpiand-type ligands.[2,23,29] To confirm this hypothesis, additional experiments were carried out by mixing a solution containing $[ZnL1]^{2+}$ (initial pH = 8) with a sodium formate/formic acid buffer solution at pH 4, so that the final solution contains a significant amount of $[ZnHL1]^{3+}$ (see Figure 6). Several experiments were carried out at different wavelengths within the 265−290 nm range, and in all cases, the only absorbance changes observed occurred within the stopped-flow mixing time, thus confirming that protonation of $[ZnL1]^{2+}$ to form $[ZnHL1]^{3+}$ is rapid in the stopped-flow time scale. Consequently, the second-order rate constant of 4.17 ± 0.05 M^{-1} s^{-1}, obtained by fitting together all the data available, corresponds to the subsequent slower decomposition of $[ZnHL1]^{3+}$.

$$k_{obs} = a[H^+] \quad (1)$$

The kinetics of decomposition of the $[CuL1]^{2+}$ complex was also studied. Solutions of Cu^{2+} and **L1** in a 1:1 molar ratio contain, at pH 7, exclusively the $[CuL1]^{2+}$ species (see Figures 4 and S6), and their UV−vis spectra show an absorption band centered at ca. 640 nm similar to that observed for other $[CuL]^{2+}$ complexes with related scorpiand-like ligands.[2,23,29] However, when these solutions are mixed with an excess of acid, the spectrum changes within the stopped-flow mixing time, so that the initial spectra in the kinetic experiments show a band at 750 nm. Thus, there is an initial rapid step whose rate

DOI: 10.1021/ic5029004
Inorg. Chem. 2015, 54, 1983−1991

Table 3. Selected Kinetic Data for the Decomposition of the Complexes Formed between Cu^{2+} and Scorpiand-Type Ligands at 298 ± 0.1 K[c]

ligand	λ_{max}[a]	c (s^{-1})[b]	b (M^{-2} s^{-1})[b]	reference
L1	750	(7.6 ± 0.8) × 10^{-6}	(6.9 ± 0.1) × 10^{-3}	this work
L2	695	(5.2 ± 0.9) × 10^{-4}	(1.16 ± 0.07)	2
L3	690	(0.8 ± 0.2) × 10^{-4}	(0.74 ± 0.03) × 10^{-3}	13
L5	730	(1.4 ± 0.6) × 10^{-4}	(3.1 ± 0.2) × 10^{-3}	22

[a]Absorption band of the intermediate formed within the stopped-flow mixing time, except for the case of **L2**, which corresponds to direct decomposition of the $[CuL]^{2+}$ complex. [b]Parameters c and b refer to eq $k_{2obs} = c + b[H^+]^2$. [c]Only species decomposing with a second-order dependence with respect to the acid are included.

constant cannot be measured with the stopped-flow technique. A similar observation has been also made for other Cu^{2+} complexes with related scorpiands, and it has been related to the conversion of $[CuL]^{2+}$ to $[CuHL]^{3+}$.[2,23,29] Nevertheless, for the other complexes, the rapid step is signaled by a shift of the band to 690 nm, which coincides with the spectrum of $[CuHL]^{3+}$ and with the spectrum of the $[CuL]^{2+}$ complex with the macrocycle lacking the pendant arm.[2,23,30] In an attempt to obtain information that could explain the different behavior of the **L1** complex, the spectrum of solutions containing Cu^{2+} and **L1** in a 1:1 molar ratio was recorded at different pH values and used to calculate the spectrum of the $[CuHL1]^{3+}$ species with the help of the speciation data. The spectrum (Figure S6, Supporting Information) is very similar to that observed for $CuL1^{2+}$ and suggests that the coordination environment of Cu^{2+} in the $[CuL1]^{2+}$ and $[CuHL1]^{3+}$ species is very similar. Moreover, stopped-flow experiments using solutions with Cu^{2+} and **L1** in a 1:1 molar ratio at an initial pH of 4, which contain a mixture of $[CuL1]^{2+}$ and $[CuHL1]^{3+}$, also show initial spectra with the band shifted to 750 nm. Thus, the different behavior of **L1** with respect to related ligands lacking the indazole ring is confirmed. The differences are essentially two: (i) conversion of $[CuL1]^{2+}$ to $[CuHL1]^{3+}$ occurs very rapidly but does not involve simply the dissociation of the donor atom in the pendant arm, and (ii) the nature of the intermediate formed within the stopped-flow mixing time in the acid-promoted dissociation of the complex is also different. Interestingly, although it clearly involves a structural reorganization more complex than the simple scorpiand-type movement observed for related ligands, the formation of the intermediate with a band at 750 nm is reversible in several cycles, as confirmed by sequential stopped-flow experiments involving the successive addition of acid and base (Figure S7, Supporting Information).

After the rapid process that occurs within the stopped flow mixing time, the intermediate generated decomposes in a slower step whose kinetics was studied using conventional UV−vis spectrophotometry. As expected from the speciation curves, this slow step leads to complete decomposition of the complex, and the spectral changes were satisfactorily fitted by a single exponential to obtain k_{2obs} values that show a second-order dependence with respect to the acid concentration (Figure S8, Supporting Information). Similar results were obtained for solutions containing $[CuL1]^{2+}$ and $[CuHL1]^{3+}$, and the values obtained from the fit by eq 2 are c = (6.9 ± 0.8) × 10^{-6} s^{-1} and b = (7.0 ± 0.1) × 10^{-3} M^{-2} s^{-1} for $[CuL1]^{2+}$ and c = (8 ± 2) × 10^{-6} s^{-1} and b = (6.8 ± 0.2) × 10^{-3} M^{-2} s^{-1} for $[CuHL1]^{3+}$. Because of the similarity of the data, the results of both sets of experiments were fitted together and yielded c = (7.6 ± 0.8) × 10^{-6} s^{-1} and b = (6.9 ± 0.1) × 10^{-3} M^{-2} s^{-1}. The rate law in eq 2 can be interpreted in terms of the classical mechanism proposed by Margerum,[31] although with the rate-determining step shifted from the breaking of the first Cu−N bond to the second one.[23] Interestingly, the $[CuL]^{2+}$ complex with the macrocycle lacking of a pendant arm (**L2**, Chart 2) also decomposes with a second-order dependence with respect to the acid, but its decomposition occurs significantly faster (see Table 3).[2]

On the other hand, decomposition of the $[CuHL]^{3+}$ species formed within the mixing time for related scorpiands typically occurs more slowly and with a first-order dependence with respect to the acid,[2,23,29] except for the case of the ligand with a pendant arm containing a 2-pyridyl group (**L3**, Chart 2), which shows a second-order dependence, although its absorption band appears at 690 nm (Table 3).[23] Formation of an intermediate with a band centered at 750 nm was observed during the decomposition of the Cu complex with the double-scorpiand receptor **L4**, but it decomposes with first-order kinetics.[32] Interestingly, an intermediate with a band at a position close (730 nm) to that observed for **L1** and decomposing with second-order kinetics was observed for the complex with another double-scorpiand receptor (**L5**) containing a pyridine spacer (Table 3).[32]

$$k_{2obs} = c + b[H^+]^2 \quad (2)$$

Although fluorescence measurements did not provide any additional information in the case of Zn^{2+}, experiments carried out for Cu^{2+} provided useful information. The data in Figure 4 show that coordination of **L1** to Cu^{2+} leads to the disappearance of the fluorescence associated with the ligand, although some fluorescence is observed at pH values between 2.5 and 5.5 because of the coexistence of the nonemissive $[CuL1]^{2+}$ with the emissive $[H_4L1]^{4+}$ species. Kinetic stopped-flow experiments with fluorescence detection were carried out using solutions containing Cu^{2+} and **L1** in a 1:1 mol ratio with the initial pH adjusted to 7.0 or 4.0, so that the decomposition of $[CuL1]^{2+}$ (pH_0 = 7.0) and a mixture of this species with Cu^{2+} and $[CuHL1]^{3+}$ (pH_0 = 4.0) could be monitored. From Figure 4, it must be expected that the initial fluorescence is very small for experiments with pH_0 = 4.0 and negligible for pH_0 = 7.0, but a fluorescence increase with time is expected to occur as the complex decomposition takes place. Surprisingly, the fluorescence experiments showed for both starting pH values the existence of a kinetic step not detected in the absorbance experiments described above. The fluorescence changes were fitted satisfactorily by a single exponential to obtain k_{obs} values that show a second-order dependence with respect to the acid concentration (Figure S9, Supporting Information), so that the fit of both series of experiments by eq 2 leads to c = 0.4 ± 0.2 s^{-1} and b = (1.72 ± 0.07) × 10^3 M^{-2} s^{-1}. It is important to note that stopped-flow experiments with simultaneous absorbance and fluorescence detection demonstrated that the fluorescence changes occur without significant changes in the absorbance so

DOI: 10.1021/ic5029004
Inorg. Chem. 2015, 54, 1983−1991

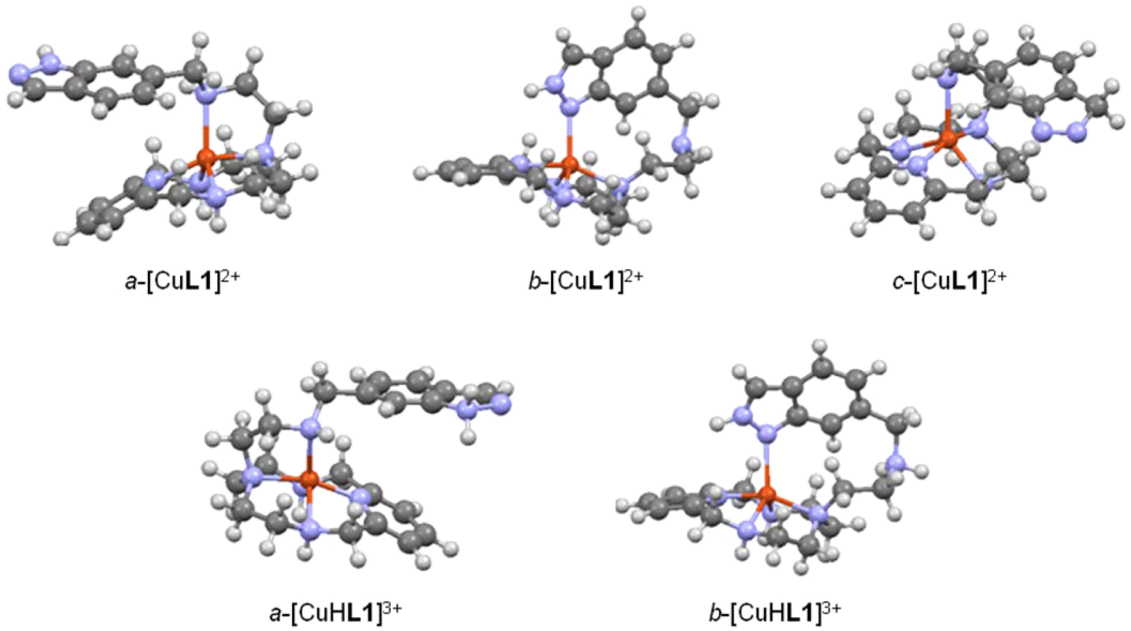

Figure 8. Optimized geometries obtained for the $[CuL1]^{2+}$ and $[CuHL1]^{3+}$ species considering the different tautomers of the indazole ring.

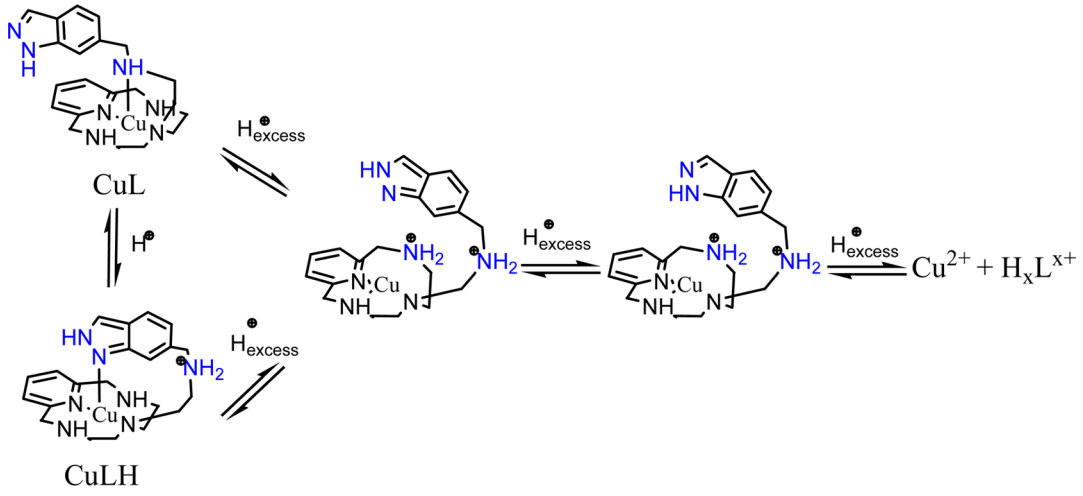

Figure 9. Proposed structural reorganization during the protonation of $[CuL1]^{2+}$ to form $[CuHL1]^{3+}$, and the subsequent protonation and tautomerization of the intermediate formed during the acid-promoted decomposition. In the conversion of $[CuL1]^{2+}$ to $[CuHL1]^{3+}$, protonation of the coordinated NH group is accompanied by tautomerization and coordination of the indazole group. In the presence of an acid excess, there is also additional rapid protonation of the macrocyclic of the macrocyclic ring and dissociation of coordinated indazole leads to an intermediate with a free 2*H*-indazole group that tautomerizes to the more stable 1*H* form.

that they cannot be associated with decomposition of the intermediate with an absorption band at 750 nm. As additional experiments in which a $[CuL1]^{2+}$ solution ($pH_0 = 7$) was mixed in the stopped-flow with a sodium formate/formic acid buffer solution at pH 4 did not show those fluorescence changes, it can be also ruled out that they are associated with the protonation of $[CuL1]^{2+}$ to form $[CuHL1]^{3+}$. At this point, DFT calculations were carried out to obtain some information that could lead to an understanding of these puzzling experimental observations.

DFT Calculations. The experiments described above indicate that $[CuL1]^{2+}$ and $[CuHL1]^{3+}$ have similar absorption spectra, which suggests that the coordination environment on the metal center is maintained upon protonation. As first protonation would likely occur at the aliphatic nitrogen of the pendant arm, which is coordinated in $[CuL1]^{2+}$, the only way to maintain the coordination environment is that one of the nitrogens in the indazole ring becomes coordinated in $[CuHL1]^{3+}$. The DFT calculations were initially aimed to explore this possibility. The starting point of the calculations was the optimization of the geometry of the $[CuL1]^{2+}$ species with the pendant arm containing the stable 1*H*-indazole form. All attempts to obtain stable geometries with coordinated 1*H*-indazole were unsuccessful, and the most stable geometry obtained was always that labeled as *a*-$[CuL1]^{2+}$ in Figure 8, which contains the Cu^{2+} ion coordinated to the four nitrogens in the macrocycle and to the aliphatic NH group in the arm. The next step was the optimization of the geometries for $[CuL1]^{2+}$ considering the 2*H*- and 3*H*-indazole tautomeric forms of **L1**. The most stable geometries so obtained are *b*-$[CuL1]^{2+}$ and *c*-$[CuL1]^{2+}$, respectively. In the case of *b*-$[CuL1]^{2+}$, the 2*H*-indazole group is coordinated to the metal center through N1, thus

DOI: 10.1021/ic5029004
Inorg. Chem. 2015, 54, 1983−1991

leading to a coordination environment that resembles that in *a*-[Cu**L1**]$^{2+}$. However, *b*-[Cu**L1**]$^{2+}$ was calculated to be 27.0 kcal mol^{-1} less stable than *a*-[Cu**L1**]$^{2+}$, and so it is not expected to be formed. In *c*-[Cu**L1**]$^{2+}$, the 3*H*-indazole group is not coordinated and the aliphatic NH group is coordinated in a way similar to that found in *a*-[Cu**L1**]$^{2+}$. However, the energy required for achieving this tautomeric form of the indazole group, *c*-[Cu**L1**]$^{2+}$ is also less stable (21.7 kcal mol^{-1}) than *a*-[Cu**L1**]$^{2+}$. Thus, the calculations indicate that *a*-[Cu**L1**]$^{2+}$ is the preferred structure for this species. This is the same coordination environment found for [CuL]$^{2+}$ complexes with related scorpiands,[2,23,29] and the observation of an absorption band at 640 nm in all cases, including *a*-[Cu**L1**]$^{2+}$, strongly suggests that this is the structure actually adopted by [Cu**L1**]$^{2+}$.

As the experimental results point to a similar coordination environment in the protonated [CuH**L1**]$^{3+}$ species, the geometries of the species resulting from protonation of *a*-[Cu**L1**]$^{2+}$ and *b*-[Cu**L1**]$^{2+}$ were also optimized, and they are labeled *a*-[CuH**L1**]$^{3+}$ and *b*-[CuH**L1**]$^{3+}$ in Figure 8.

In the *a*-[CuH**L1**]$^{3+}$ geometry, there is a protonated 1*H*-indazole group and the aliphatic NH remains coordinated, whereas, in *b*-[CuH**L1**]$^{3+}$, the aliphatic amino group is protonated and dissociated, and the 2*H*-indazole group is coordinated through N1. The *b*-[CuH**L1**]$^{3+}$ form results now to be 4.3 kcal mol^{-1} more stable than *a*-[CuH**L1**]$^{3+}$. Thus, although these relative energies must be taken with care, the whole set of calculations suggest that protonation of [Cu**L1**]$^{2+}$ occurs at the NH group in the pendant arm, but it is accompanied by tautomerization and coordination of the indazole group, as indicated in Figure 9.

CONCLUSIONS

A new scorpiand-like ligand containing an indazole moiety in its pendant arm has been synthesized. No significant differences have been observed for the acid−base behavior and the metal ion coordination when this receptor is compared with other scorpiand-like ligands previously reported. The DFT results in the previous section provide a reasonable explanation for the similarity of the UV−vis spectra of the [Cu**L1**]$^{2+}$ and [CuH**L1**]$^{3+}$ species based on the possibility of tautomerization and coordination of the indazole group in the pendant arm, thus justifying the difference with respect to related scorpiands lacking of this group. However, the experimental results indicate that, in the presence of an excess of acid, [CuH**L1**]$^{3+}$ is further protonated within the stopped-flow mixing time to form an intermediate [CuH$_x$**L1**]$^{(2+x)+}$ ($x > 1$) with a maximum at 750 nm. Given the spectral changes in the UV−vis spectrum and the low basicity of the indazole group, it is expected that the additional protonation step occurs at one of the nitrogens in the macrocycle, thus causing its dissociation and an absorption spectrum different from that of the [Cu**L2**]$^{2+}$ species. As the fluorescence and absorbance changes associated with decomposition of the intermediate with the band at 750 nm occur with very different time scales, one plausible explanation is that conversion of [CuH**L1**]$^{3+}$ to [CuH$_x$**L1**]$^{(2+x)+}$ ($x > 1$) also involves dissociation of the bond between Cu^{2+} and N1 of indazole. This process would result in formation of an intermediate containing an uncoordinated 2*H*-indazole group in the pendant arm, which would convert to the more stable 1*H*-indazole tautomer in a process signaled by fluorescence changes but that would not change the d−d bands of Cu^{2+} (see Figure 9). Once the tautomerization is completed (in less than ca. 1 s), there is the slow decomposition of the [Cu(H$_x$**L1**)]$^{(2+x)+}$ ($x > 1$) intermediate, which takes place during several hours.

As a whole, the results in this paper indicate that introduction of the indazole group in the pendant arm of a scorpiand leads to complexes that undergo reversible structural changes that involve not only the coordination−dissociation process typical of other *tren*-derived scorpiands but also coordination−dissociation and tautomerization of the indazole group. The occurrence of indazole tautomerization in coordination compounds has been previously reported, but it has not been until now that some information about its kinetics is obtained as well as its active role in the structural reorganization of metal complexes.

ASSOCIATED CONTENT

Supporting Information

Distribution diagrams, NMR spectra for the aliphatic region at different pH values, and plots of the dependence with the acid concentration of the rate constant obtained for the different Zn^{2+} and Cu^{2+} complexes. This material is available free of charge via the Internet at http://pubs.acs.org.

AUTHOR INFORMATION

Corresponding Authors

*E-mail: begona.verdejo@uv.es (B.V.).
*E-mail: enrique.garcia-es@uv.es. Phone: (+34)963544879 (E.G.-E.).
*E-mail: manuel.basallote@uca.es. Phone: +(34)956012739 (M.G.B.).

Notes

The authors declare no competing financial interest.

ACKNOWLEDGMENTS

Financial support by the Spanish Ministerio de Economía y Competitividad and FEDER funds of the European Union (Projects CONSOLIDER INGENIO CSD-2010-00065, CTQ2012-37821-C02-02, and CTQ2013-48917-C3-1-P), and Generalitat Valenciana (Project PROMETEO 2011/008) is gratefully acknowledged. B.V. wants to thank the Spanish Ministerio de Economía y Competitividad for a Juan de la Cierva Postdoctoral contract.

REFERENCES

(1) (a) Amendola, V.; Fabbrizzi, L.; Mangano, C.; Pallavicini, P. *Acc. Chem. Res.* **2001**, *34*, 488−493. (b) Lotz, T. J.; Kaden, T. A. *J. Chem. Soc., Chem. Commun.* **1977**, 15−16. (c) Lotz, T. J.; Kaden, T. A. *Helv. Chim. Acta* **1978**, *61*, 1376−1387.

(2) Verdejo, B.; Ferrer, A.; Blasco, S.; Castillo, C. E.; González, J.; Latorre, J.; Máñez, M. A.; Basallote, M. G.; Soriano, C.; García-España, E. *Inorg. Chem.* **2007**, *46*, 5707−5719.

(3) Inclán, M.; Albelda, M. T.; Frías, J. C.; Blasco, S.; Verdejo, B.; Serena, C.; Salat-Canela, C.; Díaz, M. L.; García-España, A.; García-España, E. *J. Am. Chem. Soc.* **2012**, *134*, 9644−9656.

(4) (a) Cerecetto, H.; Gerpe, A.; Gonzalez, M.; Arán, V. J.; Ochoa de Ocáriz, C. *Mini-Rev. Med. Chem.* **2005**, *5*, 869−878. (b) Thangadurai, A.; Minu, M.; Wakode, S.; Agrawal, S.; Narasimhan, B. *Med. Chem. Res.* **2012**, *21*, 1509−1523.

(5) (a) Hartinger, C. G.; Zorbas-Seifried, S.; Japukec, M. A.; Kynast, B.; Zorbas, H.; Keppler, B. K. *J. Inorg. Biochem.* **2006**, *100*, 891−904. (b) Trondl, R.; Heffeter, P.; Kowol, C. R.; Japukec, M. A.; Berger, W.; Keppler, B. K. *Chem. Sci.* **2014**, *5*, 2925−2932. (c) Kuhn, P.-S.; Pichler, V.; Rolleraaa, A.; Hejl, M.; Jakupec, M. A.; Kandioller, W.; Keppler, B. K. *Dalton Trans.* **2015**, *44*, 659−668.

DOI: 10.1021/ic5029004
Inorg. Chem. 2015, 54, 1983−1991

(6) Schmidt, A.; Beutler, A.; Snovydovych, B. *Eur. J. Org. Chem.* **2008**, 4073−4095.
(7) Rahman, A.; Malik, S.; Cun-heng, H.; Clardy, J. *Tetrahedron Lett.* **1985**, *26*, 2759−2762.
(8) Liu, Y.-M.; Yang, J.-S.; Liu, Q.-H. *Chem. Pharm. Bull.* **2004**, *52*, 454−455.
(9) Rahman, A.; Malik, S.; Hasan, S. S.; Choudhary, M. I.; Ni, C.-Z.; Clardy, J. *Tetrahedron Lett.* **1995**, *36*, 1993−1996.
(10) (a) Elguero, J.; Marzin, C.; Katritzky, A. R.; Linda, P. *The Tautomerism of Heterocycles*; Academic Press: New York, 1976. (b) Elguero, J. *Pyrazoles and Their Benzo Derivatives in Comprehensive Heterocyclic Chemistry*; Pergamon Press: Oxford, U.K., 1984; pp 291−297. (c) Elguero, J.; Katritzky, A. R.; Denisko, O. V. *Adv. Heterocycl. Chem.* **2000**, *76*, 1.
(11) Hossaini Sadr, M.; Soltani, B.; Ghao, S.; Ng, S. W. *Acta Crystallogr.* **2008**, *E64*, m109 and references therein.
(12) (a) Büchel, G. E.; Stepanenko, I. N.; Hejl, M.; Jakupec, M. A.; Keppler, B. K.; Arion, V. B. *Inorg. Chem.* **2011**, 7690−7697. (b) Büchel, G. E.; Stepanenko, I. N.; Hejl, M.; Jakupec, M. A.; Keppler, B. K.; Heffeter, P.; Berger, W.; Arion, V. B. *J. Inorg. Biochem.* **2012**, *113*, 47−54.
(13) García-España, E.; Ballester, M.-J.; Lloret, F.; Moratal, J. M.; Faus, J.; Bianchi, A. *J. Chem. Soc., Dalton Trans.* **1988**, 101−104.
(14) Fontanelli, M.; Micheloni, M. Program for the automatic control of the microburette and the acquisition of the electromotive force readings (PASAT). *Proceedings of the I Spanish-Italian Congress on Thermodynamics of Metal Complexes*, Peñíscola, Castellón, Spain, 1990.
(15) (a) Gran, G. *Analyst* **1952**, *77*, 661−671. (b) Rossotti, F. J.; Rossotti, H. *J. Chem. Educ.* **1965**, *42*, 375−378.
(16) Gans, P.; Sabatini, A.; Vacca, A. *Talanta* **1996**, *43*, 1739−1753.
(17) (a) Glasoe, P. K.; Long, F. A. *J. Phys. Chem.* **1960**, *64*, 188−190. (b) Covington, A. K.; Paabo, M.; Robinson, R. A.; Bates, R. G. *Anal. Chem.* **1968**, *40*, 700−706.
(18) Binstead, R. A.; Jung, B.; Zuberbühler, A. D. *SPECFIT-32*; Spectrum Software Associates: Chapel Hill, NC, 2000.
(19) Frisch, M. J.; Trucks, G. W.; Schlegel, H. B.; Scuseria, G. E.; Robb, M. A.; Cheeseman, J. R.; Scalmani, G.; Barone, V.; Mennucci, B.; Petersson, G. A.; Nakatsuji, H.; Caricato, M.; Li, X.; Hratchian, H. P.; Izmaylov, A. F.; Bloino, J.; Zheng, G.; Sonnenberg, J. L.; Hada, M.; Ehara, M.; Toyota, K.; Fukuda, R.; Hasegawa, J.; Ishida, M.; Nakajima, T.; Honda, Y.; Kitao, O.; Nakai, H.; Vreven, T.; Montgomery, J. A., Jr.; Peralta, J. E.; Ogliaro, F.; Bearpark, M.; Heyd, J. J.; Brothers, E.; Kudin, K. N.; Staroverov, V. N.; Kobayashi, R.; Normand, J.; Raghavachari, K.; Rendell, A.; Burant, J. C.; Iyengar, S. S.; Tomasi, J.; Cossi, M.; Rega, N.; Millam, J. M.; Klene, M.; Knox, J. E.; Cross, J. B.; Bakken, V.; Adamo, C.; Jaramillo, J.; Gomperts, R.; Stratmann, R. E.; Yazyev, O.; Austin, A. J.; Cammi, R.; Pomelli, C.; Ochterski, J. W.; Martin, R. L.; Morokuma, K.; Zakrzewski, V. G.; Voth, G. A.; Salvador, P.; Dannenberg, J. J.; Dapprich, S.; Daniels, A. D.; Farkas, Ö.; Foresman, J. B.; Ortiz, J. V.; Cioslowski, J. D.; Fox, J. *Gaussian 09*, Revision C.01; Gaussian, Inc.: Wallingford, CT, 2009.
(20) Schaftenaar, G.; Noordik, J. H. *J. Comput.-Aided Mol. Des.* **2000**, *14*, 123−134.
(21) (a) Becke, A. D. *J. Chem. Phys.* **1988**, *88*, 2547−2549. (b) Becke, A. D. *Phys. Rev. A* **1988**, *38*, 3098−3100. (c) Becke, A. D. *J. Chem. Phys.* **1993**, *98*, 5648−5652.
(22) Krishnan, R.; Binkley, J. S.; Seeger, R.; Pople, J. A. *J. Chem. Phys.* **1980**, *72*, 650−654.
(23) Blasco, S.; Verdejo, B.; Clares, M. P.; Castillo, C. E.; Algarra, A. G.; Latorre, J.; Mañez, M. A.; Basallote, M. G.; Soriano, C.; García-España, E. *Inorg. Chem.* **2010**, *49*, 7016−7027.
(24) Clares, M. P.; Blasco, S.; Inclán, M.; del Castillo Agudo, L.; Verdejo, B.; Soriano, C.; Doménech, A.; Latorre, J.; García-España, E. *Chem. Commun.* **2011**, *47*, 5988−5990.
(25) (a) Berden, G.; Meerts, W. L.; Jalviste, E. *J. Chem. Phys.* **1995**, *103*, 9596−9606. (b) Stadlbauer, W. Web page: http://www-och.kfunigraz.ac.at/~sta/pub/086/086.pdf.
(26) (a) Bernardo, M. A.; Pina, F.; Escuder, B.; García-España, E.; Godino-Salido, M. L.; Latorre, J.; Luis, S. V.; Ramírez, J. A.; Soriano, C. *J. Chem. Soc., Dalton Trans.* **1999**, 915−921. (b) Czarnik, A. W. *Acc. Chem. Res.* **1994**, *27*, 302−307. (c) Czarnik, A. W. *Fluorescent Chemosensors for Ion and Molecule Recognition*; American Chemical Society: Washington, DC, 1992.
(27) Bernardo, M. A.; García-España, E.; Latorre, J.; Luis, S. V.; Llinares, J. M.; Pina, F.; Ramírez, J. A.; Soriano, C. *Inorg. Chem.* **1998**, *37*, 3935−3942.
(28) (a) Díaz, P.; Basallote, M. G.; Máñez, M. A.; García-España, E.; Gil, L.; Latorre, J.; Soriano, C.; Verdejo, B.; Luis, S. V. *Dalton Trans.* **2003**, 1186−1193. (b) Aguilar, J.; Basallote, M. G.; Gil, L.; Hernández, J. C.; Máñez, M. A.; García-España, E.; Soriano, C.; Verdejo, B. *Dalton Trans.* **2004**, 94−103. (c) Verdejo, B.; Basallote, M. G.; Ferrer, A.; Mañez, M. A.; Hernández, J. C.; Chadim, M.; Hodacova, J.; Llinares, J. M.; Soriano, C.; García-España, E. *Eur. J. Inorg. Chem.* **2008**, 1497−1507. (d) Algarra, A. G.; Basallote, M. G.; Castillo, C. E.; Clares, M. P.; Ferrer, A.; García-España, E.; Llinares, J. M.; Máñez, M. A.; Soriano, C. *Inorg. Chem.* **2009**, *48*, 902−914. (e) Mendoza, A.; Aguilar, J.; Basallote, M. G.; Gil, L.; Hernández, J. C.; Máñez, M. A.; García-España, E.; Ruiz-Ramírez, L.; Soriano, C.; Verdejo, B. *Chem. Commun.* **2003**, 3032−3033.
(29) Castillo, C. E.; Máñez, M. A.; Basallote, M. G.; Clares, M. P.; Blasco, S.; García-España, E. *Dalton Trans.* **2012**, *41*, 5617−5624.
(30) Costa, J.; Delgado, R. *Inorg. Chem.* **1993**, *32*, 5257−5265.
(31) (a) Cabbiness, D. K.; Margerum, D. W. *J. Am. Chem. Soc.* **1969**, *91*, 6540−6541. (b) Read, A.; Margerum, D. W. *Inorg. Chem.* **1981**, *20*, 3143−3149.
(32) Castillo, C. E.; González-García, J.; Llinares, J. M.; Máñez, M. A.; Jiménez, H. R.; García-España, E.; Basallote, M. G. *Dalton Trans.* **2013**, *42*, 6131−6141.

DOI: 10.1021/ic5029004
Inorg. Chem. 2015, 54, 1983−1991